AIAA SciTech Forum
12-16 January 2026, Orlando, FL
AIAA SCITECH 2026 Forum

10.2514/6.2026-0943

Comparative Study of Zero-Net Mass Flux Flow Control Airfoils Using Fluidic Actuators

Joshua Prabahar * Gecheng Zha †
Dept. of Mechanical and Aerospace Engineering
University of Miami, Coral Gables, Florida 33124

Abstract

This paper examines four different active flow control (AFC) airfoils employing fluidic actuators in a zero net mass flux configuration. Modifications to the base NACA 6421 airfoil are made to achieve the four AFC airfoil configurations. Suction and injection slots, positioned at different locations and orientations on the upper surface, provide the means of fluidic actuation. Computational fluid dynamics (CFD) simulations are conducted using the in-house FASIP CFD code, which is a validated RANS solver incorporating the Spalart-Allmaras (SA) turbulence model, a third-order WENO scheme for inviscid fluxes, and second-order central differencing for viscous terms. The investigation is conducted at a Mach number (M) of 0.10 and a Reynolds number R_e of 2.6×10^6 under a simulated cruise conditions. Comparison with the baseline NACA 6421 airfoil demonstrate significant enhancements in lift and drag performance in three of the four AFC configurations studied. Examination of the isentropic Mach number plots reveal that having the suction slot located downstream of the suction peak, such as in AFC2 and AFC4, demonstrate lower power requirements than the configuration with the suction slot positioned in the vicinity of the suction peak, AFC1. Force component analysis conducted on all airfoils indicates a significant benefit of the jet reactionary force applied to airfoils with injection slots downstream of the suction slot, although the extent of this benefit may depend on the proximity to the suction slot and to the trailing edge. Furthermore, it is noted that AFC4, the configuration representing the Co-Flow Jet (CFJ), has the highest lift enhancement by airfoil circulation augmentation, substantially larger than AFC1, AFC2, and AFC3, however, the position and orientation of the suction slot reduces the overall lift increment. Both AFC2 and AFC4 achieve peak aerodynamic efficiency at relatively lower AoA of $\alpha = 10°$ and $\alpha = 5°$, respectively, with AFC2 and AFC4 achieving the highest efficiencies of $(C_L/C_D)_c = 91.91$ and $(C_L/C_D)_c = 89.56$ respectively. AFC1 achieves higher airfoil productivity values although at higher AoA than the alternative configurations, achieving the highest value of $(C_L^2/C_D)_c = 192.93$ at $\alpha = 20°$. AFC2 demonstrates the highest effectiveness gain over the baseline NACA6421. It also has the highest efficiency gain, except at $\alpha = 5°$ at which point AFC4 peaks before steadily declining. AFC1 steadily increases in both effectivenss gain and efficiency gain until $\alpha = 15°$. However, AFC3 is less effective and efficient than the baseline NACA6421 airfoil until $\alpha = 10°$.

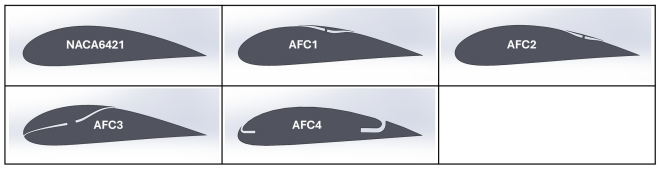

Figure 1: Summary of 2D AFC configurations used in current study

* Ph.D. Student
† Professor, ASME Fellow, AIAA associate Fellow

Nomenclature

AFC	Active Flow Control
BLC	Boundary Layer Control
CC	Circulation Control
PFC	Passive Flow Control
CFJ	CoFlow jet
SST	Suction Surface Translation
$AoA(\alpha)$	Angle of attack
LE	Leading Edge
TE	Trailing Edge
c	Profile chord
U	Flow velocity
q	Dynamic pressure $0.5\,\rho\,U^2$
p	Static pressure
T	Static temperatue
ρ	Air density
μ	Dynamic viscosity
R	Specific gas constant
P	Pumping power
C_L	Lift coefficient $L/(q_\infty\,S)$
C_D	Drag coefficient $D/(q_\infty\,S)$
C_μ	Jet momentum coef. $\dot{m}_j\,U_j/(q_\infty\,S)$
Pc	Power coefficient $P/(q_\infty\,S\,V_\infty)$
$(C_L/C_D)_c$	AFC airfoil corrected efficiency $C_L/(C_D$+Pc)
R_e	Reynolds number
M	Mach number
c_p	Constant pressure specific heat
γ	Air specific heats ratio
T_t	Total temperature
P_t	Total pressure
Γ	Total pressure ratio
H_t	Total specific enthalpy
$\dot{m}$	Mass flow across the pump
$_\infty$	Subscript, stands for free stream
$_j$	Subscript, stands for jet

1 Introduction

Optimization of modern commercial and military aircraft performance is governed by enhancements in lift, reduction in drag, separation delay, and noise suppression while maintaining a stable operating condition[1]. A primary focus tends to be placed on increasing lift, reducing drag and mitigating separation in take-off and landing, where a high lift at low speeds is required. The importance in achieving said requirements is given by the empirical cost-benefits presented in Table 1. However, for any means of increasing the maximum lift coefficient, it is desirable not to reduce the efficiency at cruise. Passive and active flow control methods have been investigated to improve aircraft performance. Passive flow control

(PFC) is low cost, reduces complexity, and has minimal energy requirement, making it generally more practical for application. Such examples include the use of riblets, large eddy breakup devices (LEBU) such as plates or fences, vortex generators, rippled trailing edges, streamwise corrugations, contour shaping, and variable geometry via slats and flaps[1, 2, 3]. However, slats and flaps tend to carry an added weight and drag penalty for the added lift.

Table 1: Empirical Cost Benefits of Enhanced Lift Performance [4]

Aerodynamic Performance	Cost Benefit
5% increase in takeoff C_L, max	12-15% increase in payload
5% increase in takeoff L/D	20% increase in payload
5% increase in landing C_L, max	25% increase in payload

As passive flow control was considered to approach a limit in the 1950s, it was understood that further lift increases could only be achieved by adding energy to the flow[2, 5] via active flow control (AFC) methods. AFC traces its origins to the understanding of the boundary layer separation by the work of Prandtl in 1904, where he described that as the fluid experiences an increase in pressure in the boundary layer, the kinetic energy is then partially converted to potential energy[6]. The resulting deficient kinetic energy then becomes insufficient to overcome the high adverse pressure gradient, and hence is deflected laterally, transitioning the flow to turbulence and separation. This fundamental understanding of the boundary layer flow behavior gave rise to the beginning of boundary layer control (BLC) methods. Later, the inception of the important quantity of the momentum coefficient by Poisson-Quinton (1948)[7] was defined to quantify the jet momentum added to the flow. When a critical jet momentum supplied generated a lift coefficient greater than that predicted by potential flow theory, supercirculation was considered to occur. This led to the study of circulation control (CC) that involved the redistribution of stagnation pressure points due to jet actuation[8]. Active flow control then encompasses both BLC and CC in a broader view in that it energizes a flow field so that it produces greater lift, reduced drag, and delays separation. Yang and Zha (2017)[9] presented an alternative quantitative concept that describes the superseding of the maximum lift coefficient predicted by potential flow theory as the concept of super lift coefficient.

Numerous studies of AFC implementations have been studied and well-documented, which include the externally blown flap (as seen in the McDonnell Douglas YC-15 [5]), internally blown Coanda flap (as seen in the Lockheed F-104 Starfighter), tangentially blown jets or suction [10](as seen in CC wing of A-6 flight demonstrator [8]), suction slots, moving airfoil wall (such as rotating cylinder or endless belt), surface-mounted actuators such as synthetic jets [11], plasma-based or acoustic-based actuators [12], pulsed vortex generators [13], and more recently sweeping jets (fluidic oscillators) as part of the Boeing 757 ecoDemonstrator testbed [14]. Interest in AFC has developed to the point that it is also being studied as a replacement for traditional control surfaces via the DARPA X-65 program. Xu and Zha [15] applied CoFlow Jet AFC to enhance aircraft vertical tail control surface with low energy expenditure. However, according to Greenblatt et al(2019)[16], AFC becomes viable only when a decisive aerodynamic advantage can be demonstrated over passive flow control techniques.

A key consideration of major importance is energy expenditure. When the aerodynamic efficiency gain outweighs the energy expenditure (power required) of the active flow control method from a system perspective, the method may be considered to have a net benefit. Additionally, conversion efficiency of the different actuators must be considered; however, this is a function of the actuator type, scaling, and manufacturer making it generally more difficult to reasonably and accurately quantify and, as such, will be excluded from this investigation. From the fluid mechanics point of view, the power required is an independent measure of merit indicating how much power is needed to achieve the flow control effect and

hence can still be studied in the absence of the actual actuator unit.

Xu et al. [17] presented three measures of merits of AFC (MoMs): 1) effectiveness, 2) power required (PR), and 3) power conversion efficiency (PCE). Effectiveness quantifies performance enhancement, for example, removal of flow separation, drag reduction, lift increase, stall prevention, noise mitigation, etc. Power required quantifies the AFC power needed to achieve the targeted effectiveness. Power conversion efficiency quantifies the efficiency to convert the external power (e.g. mechanical, electric, and chemical) to the power required by the controlled flow. It determines how much total power the actual flow control system will be consume. Xu and Zha [18] conducted the first exergy analysis demonstrating that co-flow jet (CFJ) active flow control can not only eliminate flow separation and distortion of a serpentine duct (S-duct), but also leverage the energy state of the inlet system with the available work increased more than the CFJ energy consumed.

Only a very small number of studies apply AFC to improve cruise efficiency at low angle of attack (AoA). This is because it is very difficult to improve the efficiency of benign flows that are far from stall at low AoA. Improving cruise efficiency requires the AFC to have high merits for all the three MoMs. Lefebvre et al. [19][20] first incorporated the energy expenditure of the Coflow Jet (CFJ) AFC into the aircraft aerodynamic efficiency for cruise. One factor that facilitates the incorporation of the required power of the CFJ AFC into the overall aerodynamic efficiency is its zero-net-mass-flux (ZNMF) characteristic, which enables an accurate and well-defined calculation of the power required. The productivity efficiency was also first introduced in [9].

The purpose of this paper is to conduct a preliminary numerical investigation of cruise efficiency for several ZNMF AFC airfoils, including the previously studied CFJ airfoil. The ZNMF condition is defined based on a two-dimensional control volume enclosing the controlled flow in the streamwise plane [21].

The widely studied CC airfoil employs flow injection only and therefore does not satisfy the ZNMF definition. Consequently, the CC airfoil is not included in this study, as its required power is difficult to quantify and depends on the flow path that is unknown.

The performance of an AFC airfoil could be sensitive to detailed configuration parameters, including the size, location, and orientation of the injection and suction slots. The AFC configurations considered in this paper are based on our limited trade studies and are not optimized. As a result, the findings presented herein should be regarded as preliminary references rather than definitive conclusions. In addition, the numerical results presented in this paper have not yet been validated by experimental data.

Finally, this study investigates only two of the three MoMs: effectiveness and power required. The third MoM, external energy conversion efficiency, is not considered because it depends on the specific AFC actuator technology employed. In other words, the conversion efficiency of all the AFC actuators studied are assumed to be 100%. Different actuator types can exhibit substantially different energy conversion efficiencies, which would ultimately determine the system efficiency and benefit. The detailed assessment of different AFC actuators should be a separate study.

2 Airfoil Configurations

As shown in Fig. 1, the baseline NACA 6421 airfoil and four AFC airfoils are studied in this paper. Actuation is performed through suction and injection slots connected by an embedded compressor/actuator (although not illustrated) that acts as an energy source. Both suction and injection slots are simultaneously incorporated into each configuration such that any mass flux removed by the suction slot is reintroduced by the injection slot to ensure that a ZNMF condition is maintained. Since the idealized geometric form of each AFC configuration is unknown at this time, geometric constraints are prescribed based on trade studies. This prescribes the suction and injection slot height to be $0.65\%c$ for 3 of the 4 AFC configurations. The fourth configuration is extracted directly as the CFJ6421-SST150-SUC247-

INJ117 airfoil which is presented in a previous study[22]. This prescribes the suction slot height to be 2.47%c and the injection slot height to be 1.17%c. It is of note that the internal duct passages of each configuration have been adjusted independently to create a near uniform velocity distribution. The details of each AFC airfoil configuration are described below.

2.1 AFC1: Suction Slot near LE, Injection Slot near Mid-Chord

As shown in Figure 1, AFC1 has the suction slot at $0.327c$ from the LE on the suction surface and the injection slot placed downstream at $0.627c$ blown tangentially to create an internal jet-blown flap. This configuration is adapted from the geometry presented by Zengjunz et al.(2010)[23] with the micro-pore membranes replaced with slots as shown in Figure 2. Initial trials were conducted that compared the performance of using a pure jet flap to that of an internally blown jet flap without flap deflection. It was found that from an aerodynamic perspective, the internally blown jet flap had enhanced performance over the jet flap. This is in agreement with the C_L and C_D plots of Gainer et al.(1976)[24] when interpolated for the same momentum coefficient.

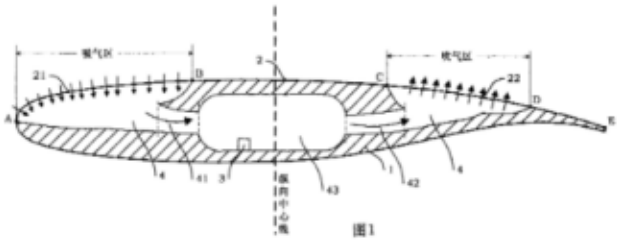

Figure 2: Airfoil profile as presented in [23]

2.2 AFC2: Suction Slot near Mid-Chord , Injection Slot near TE

As shown in Figure 1, AFC2 has the suction and injection slots are placed $0.600c$ and $0.800c$ from the LE respectively. The geometry is made to mimic an embedded crossflow fan as seen in Figure 3, although in a simplified manner. This implementation is adapted from the geometries presented by Perry and Ansell(2017)[25] and Kim and Saunders(2003)[26] as seen in Figure 3. Investigations involving a crossflow fan typically define a rotational speed; however, to simplify the geometry and ensure that it is consistent with the other AFC configurations, the fan itself is not simulated. Rather, as with all AFC configurations, a momentum coefficient is specified that would represent the pressure rise across the crossflow fan. As such, the rotation or swirl velocity introduced by the fan are neglected for this study. The injection slot is made to blow over the surface of an undeflected flap as described for AFC1.

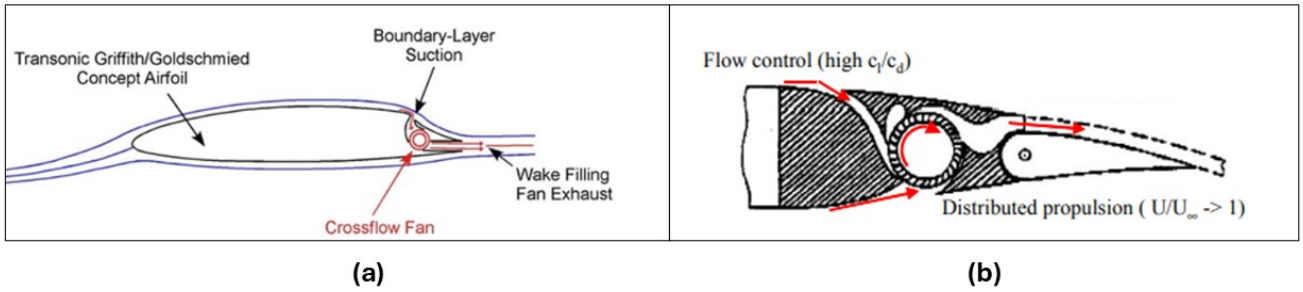

Figure 3: Airfoil profile as presented in [25](a) [26](b)

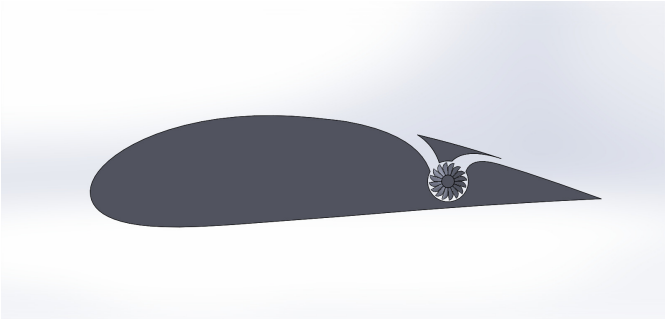

Figure 4: Representative airfoil combining implementations of [25] and [26]

2.3 AFC3: Suction Slot at LE, Injection Slot at Mid-Chord

As shown in Figure 1, AFC3 has the suction slot placed at the very LE and the injection slot placed at $0.5c$ from the LE. Initial trials indicated a negative impact in having the injection slot a significant distance away from the suction slot. Hence, the injection slot is placed at the mid-chord as opposed to close to the TE. The jet injection slot is made to blow over the surface of an undeflected flap as described for AFC1.

2.4 AFC4: CoFlow Jet (CFJ) airfoil

The CFJ is a well-studied AFC technology with ultra-high lift capabilities and cruise efficiency with low energy expenditure when integrated into an airfoil[9, 21, 27, 28, 29, 30, 31, 32, 33, 34, 35, 36, 37, 38, 39, 40]. It withdraws a small quantity of the mass flow near the TE, pressurizes it, and ejects it tangent to the airfoil surface near the LE, as seen in Figure 5, which energizes the boundary layer and keeps the flow attached under extreme adverse pressure gradients[41, 42]. The AFC4 is adopted from the configuration in a previous study [22].

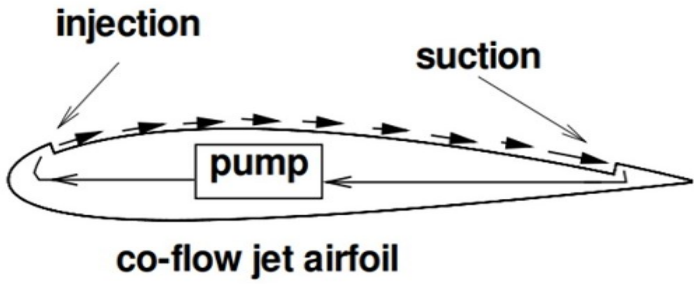

Figure 5: Sketch of CoFlow Jet airfoil

Table 2: AFC configurations - geometric summary

Airfoil	Inj. size (%c)	Suc. size (%c)	Inj. position (c)	Suc. position (c)
NACA 6421	-	-	-	-
AFC1	0.65	0.65	0.627	0.327
AFC2	0.65	0.65	0.800	0.600
AFC3	0.65	0.65	0.500	0.000
AFC4	1.17	2.47	0.020	0.800

The CFJ airfoil adopted from [22] for this study has the injection slot size of 1.17%c. The trade study conducted by Ding, et al [43] indicates that the same CFJ airfoil with reduced injection size of 0.65%c at a high freestream Mach number of 0.17 increases the productivity efficiency.

3 AFC Parameters

3.1 Lift and Drag Calculation

The momentum and pressure at the injection and suction slots produce a reactionary force, which must be included in CFD simulation. Using control volume analysis, the reactionary force can be calculated using the flow parameters at the injection and suction slot opening surfaces. Zha et al. [27] give the following formulations to calculate the lift and drag due to the jet reactionary force for a AFC airfoil. By considering the effects of injection and suction jets on the ZNMF AFC airfoil, the expressions for these reactionary forces are given as :

$$F_{x_{AFC}} = (\dot{m}_j V_{j1} + p_{j1} A_{j1}) * cos(\theta_1 - \alpha) - (\dot{m}_j V_{j2} + p_{j2} A_{j2}) * cos(\theta_2 + \alpha) \tag{1}$$

$$F_{y_{AFC}} = (\dot{m}_{j1} V_{j1} + p_{j1} A_{j1}) * sin(\theta_1 - \alpha) + (\dot{m}_{j2} V_{j2} + p_{j2} A_{j2}) * sin(\theta_2 + \alpha) \tag{2}$$

where the subscripts 1 and 2 stand for the injection and suction respectively, and θ_1 and θ_2 are the angles between the injection and suction slot's surface and a line normal to the airfoil chord[27]. α is the angle of attack.

The total lift and drag on the airfoil can then be expressed as:

$$D = R'_x - F_{x_{AFC}} \tag{3}$$

$$L = R'_y - F_{y_{AFC}} \tag{4}$$

where R'_x and R'_y are the surface integral of pressure and shear stress in x (drag) and y (lift) direction excluding the internal ducts of injection and suction.

3.2 Jet Momentum Coefficient

The jet momentum coefficient C_μ is a parameter used to quantify the jet intensity. It is defined as:

$$C_\mu = \frac{\dot{m}V_j}{\frac{1}{2}\rho_\infty {V_\infty}^2 S} \tag{5}$$

where $\dot{m}$ is the injection mass flow, V_j is the mass-averaged injection velocity, ρ_∞ and V_∞ denote the free stream density and velocity, and S is the planform area. In 2D, planform area, S, reduces to the aerodynamic chord, c.

3.3 Fluidic Actuator Power Coefficient

AFC in this study is implemented by mounting a fluidic pumping system inside the wing that withdraws air from the suction slot and blows it into the injection slot. The power consumption is determined by the jet mass flow and total enthalpy change as the following:

$$P = \dot{m}(H_{t1} - H_{t2}) \tag{6}$$

where H_{t1} and H_{t2} are the mass-averaged total enthalpy in the injection cavity and suction cavity respectively, P is the Power required by the pump and $\dot{m}$ the jet mass flow rate. Introducing P_{t1} and P_{t2} as the mass-averaged total pressure in the injection and suction cavity respectively, the fluidic actuator efficiency η, and the total pressure ratio of the pump $\Gamma = \frac{P_{t1}}{P_{t2}}$, the power consumption is expressed as:

$$P = \frac{\dot{m}C_p T_{t2}}{\eta}(\Gamma^{\frac{\gamma-1}{\gamma}} - 1) \tag{7}$$

where γ is the specific heat ratio equal to 1.4 for air , C_p is the specific heat at constant pressure, T_t is the total pressure at the suction slot, η is the AFC fluidic actuator efficiency. The power coefficient is expressed as:

$$P_c = \frac{P}{\frac{1}{2}\rho_\infty V_\infty^3 S} \tag{8}$$

In this study, all the fluidic actuators' efficiency, η, is assumed to be 100%. Therefore, the power calculated by Eq. 7 is the required power to achieve the fluid mechanics effect instead of the actual power.

3.4 Aerodynamic Efficiency

The conventional wing aerodynamic efficiency is defined as:

$$\frac{C_L}{C_D} \tag{9}$$

For the AFC airfoils, the ratio above still represents the pure aerodynamic relationship between lift coefficient and drag coefficient. However, since active flow control methods consumes energy, the ratio

above is modified to take into account the energy consumption of the fluidic actuator. The formulation of the corrected aerodynamic efficiency for AFC airfoils is given in Eqn.10.

$$(\frac{C_L}{C_D})_c = \frac{C_L}{C_D + P_c} \tag{10}$$

If the fluidic actuator power coefficient is set to 0, Eqn.10 returns to the aerodynamic efficiency of a conventional airfoil.

3.5 Aerodynamic Productivity

In order to more informatively describe the performance of high-lift airfoils, the concept of aerodynamic productivity efficiency, defined as C_L^2/C_D, is introduced [9]. This is a more comprehensive parameter than the conventional aerodynamic efficiency C_L/C_D to measure the merit of an aircraft aerodynamic design for cruise performance. The former includes not only the information of C_L/C_D, but also the information of the aircraft weight C_L. For example, for two aircraft designs having the same C_L/C_D with one C_L twice larger than the other, if the wing sizes are the same, one airplane will be able to carry twice more weight than the other with productivity and wing loading increased by 100%. Such a large difference is not reflected by C_L/C_D, but very well reflected by C_L^2/C_D.

$$(\frac{C_L^2}{C_D})_c = \frac{C_L^2}{(C_D + Pc)} \tag{11}$$

4 CFD Simulation Setup

4.1 CFD Code

The in house FASIP(Flow-Acoustics-Structure Interaction Package) CFD code is used to conduct the numerical simulation. The 2D Reynolds Averaged Navier-Stokes (RANS) equations with one-equation Spalart-Allmaras(SA) turbulence model was used. A 3rd order WENO scheme for the inviscid flux [44, 45, 46, 47, 48, 49] and a 2nd order central differencing for the viscous terms [44, 48] are employed to discretize the Navier-Stokes equations. The low diffusion E-CUSP scheme used as the approximate Riemann solver suggested by Zha et al [45] is utilized with the WENO scheme to evaluate the inviscid fluxes. Implicit time marching method using Gauss-Seidel line relaxation is used to achieve a fast convergence rate [50]. Parallel computing is implemented to save wall clock simulation time [51].The FASIP CFD code and its numerical algorithms are intensively validated with CoFlow Jet flows [27, 30, 52, 53, 54, 55].

4.2 Boundary Conditions

The 3rd order accuracy no slip condition is enforced on the solid surface with the wall treatment suggested in [56] to achieve the flux conservation on the wall. The far field boundary is located at $100c$ with an O-mesh topology. Total pressure, total temperature, and flow angles are specified at the upstream portion of the far field. Constant static pressure is applied at the downstream portion of the far field. The first grid point on the airfoil surface is placed at $y^+ \approx 1$.

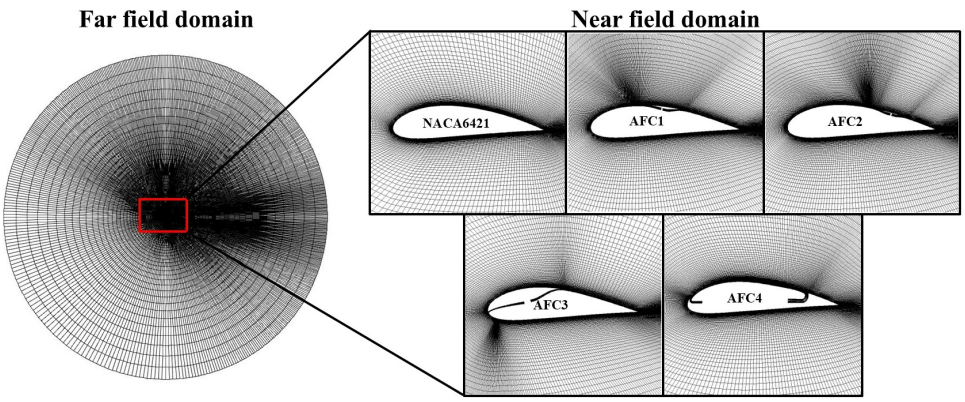

Figure 6: Computational mesh of AFC configurations of current study

4.3 Mesh Refinement

For the purpose of assessing the mesh refinement applied to the different AFC airfoils, the 10° AoA flow condition is selected for comparison. The momentum coefficient, C_μ, for each configuration is set based on the optimal aerodynamic efficiency point at that particular AoA as presented later in the results. Comparisons are made based on the percentage difference in C_L, C_D and P_C compared to the average result of that AFC configuration.

Table 3: AFC Mesh Refinement Results

Identifier	mesh	# of nodes	C_μ	C_L	C_D	P_C	C_L % diff	C_D% diff	P_C % diff
NACA6421	coarse	24300	-	1.4236	0.0359	-	1.2%	6.6%	-
	medium	48300	-	1.3960	0.0330	-	0.7%	2.1%	-
	fine	96300	-	1.3991	0.0322	-	0.5%	4.5%	-
AFC1	coarse	43637	0.025	1.8777	0.0123	0.0144	0.1%	7.3%	1.7%
	medium	104356	0.025	1.8802	0.0104	0.0149	0.2%	8.9%	1.8%
	fine	206316	0.025	1.8722	0.0116	0.0146	0.2%	1.6%	0.1%
AFC2	coarse	43637	0.015	1.9143	0.0116	0.0101	0.1%	3.9%	1.3%
	medium	104356	0.015	1.9180	0.0103	0.0106	0.3%	7.8%	3.6%
	fine	206316	0.015	1.9038	0.0116	0.0100	0.4%	3.9%	2.4%
AFC3	coarse	37157	0.025	1.5983	0.0242	0.0092	0.3%	1.6%	4.8%
	medium	91476	0.025	1.5923	0.0233	0.0087	0.0%	2.2%	1.4%
	fine	180636	0.025	1.5884	0.0240	0.0085	0.3%	0.7%	3.4%
AFC4	coarse	37459	0.060	1.9352	0.0111	0.0153	0.2%	6.6%	15.0%
	medium	74279	0.060	1.9392	0.0101	0.0124	0.1%	2.7%	7.0%
	fine	147919	0.060	1.9401	0.0100	0.0123	0.1%	3.9%	7.9%

As seen in Table 3, with the exception of the coarse mesh of the NACA6421 airfoil, all C_L results are within 1% of the average. The difference in P_C is dependent on the particular configuration. AFC1 has relatively low deviations in P_C, while AFC4 has the highest deviations, within which the medium and fine mesh are significantly closer in actual value. C_D has generally higher deviations than C_L and P_C, however, this is expected due to the difficulty in predicting drag. The largest deviation between maximum and minimum C_D is observed in the NACA6421 airfoil with 4 counts difference compared to

1 or 2 counts for the AFC configurations. As P_C is a critical parameter for efficiency calculations, the medium and fine mesh demonstrate better consistency when examining the AFC configuration with the highest deviation, AFC4, therefore, the medium mesh is selected to be used for this study to balance computational efficiency.

It is noted that the mesh sizes of AFC1, AFC2, and AFC3 are generally larger than that of AFC4. This is because more mesh points are required to resolve the jet in the wake region behind the TE resulting from the orientation and position of the slots of these configurations.

4.4 Simulation Cases

Table 4 provides the freestream conditions computed in this study. AoA (α) is varied from 0° to 30° for AFC1 and AFC4 in increments as follows: 0°, 2°, 5°, 10°, 15°, 20°, and 30°. The baseline NACA 6421 is stalled beyond AoA of 20°. AFC2 and AFC3 cannot achieve attached flow at AoA of 30° and therefore no results are presented. The jet momentum coefficient, C_μ, is varied such as to achieve the highest aerodynamic efficiency, $(C_L/C_D)_c$, within a resolution of $C_\mu = \pm\ 0.005$. The Reynolds number is obtained from a previous study using the same AFC configuration as AFC4 [22].

Table 4: Simulation cases used in the current study

Airfoil	Mach	Re	AoA
NACA 6421	0.10	2.6×10^6	0°-20°
AFC1	0.10	2.6×10^6	0°-30°
AFC2	0.10	2.6×10^6	0°-20°
AFC3	0.10	2.6×10^6	0°-20°
AFC4	0.10	2.6×10^6	0°-30°

5 Results and Discussion

The 2D simulation given the flow conditions of Table 4 provide meaningful insights into the flow behavior and aerodynamic performance for each of the AFC airfoils investigated. Figure 7 and Figure 8 are the resulting flow fields of each AFC airfoil at $\alpha = 10°$ under optimal $(C_L/C_D)_C$ condition, the corresponding C_μ values of which are given in Table 6 of the appendix. From observation of the flow field it can be seen that at $\alpha = 10°$, the flow of the baseline NACA6421 airfoil begins to separate towards the TE. With the addition of AFC to the airfoil, the flow is able to be reattached but to different degrees. AFC1 and AFC2 have fully accelerated flows on the suction surface. In contrast, AFC3 has a low momentum flow towards the TE, although the flow remains attached as seen in Figure 8a. This may be due to the injection slot being significantly upstream of the TE combined with a low C_μ value.

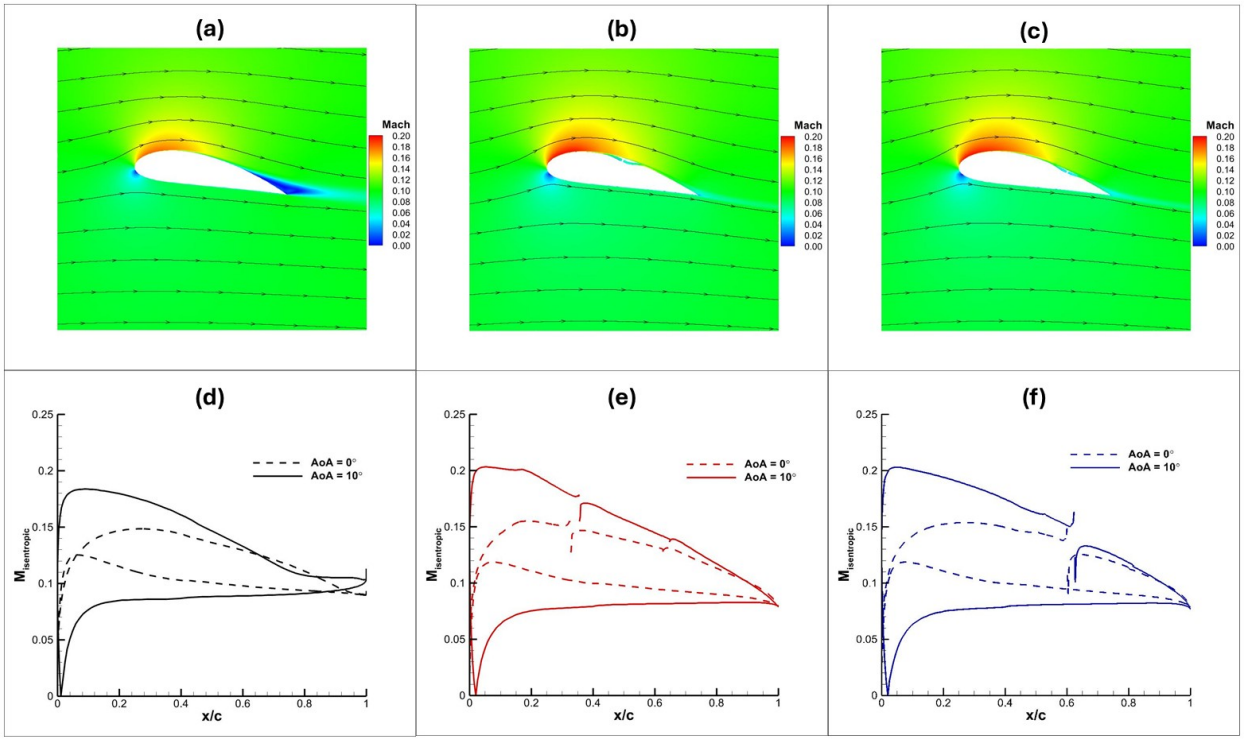

Figure 7: Flow field and corresponding isentropic Mach number surface plot for 2D NACA 6421, AFC1 and AFC2 for $\alpha = 10°$

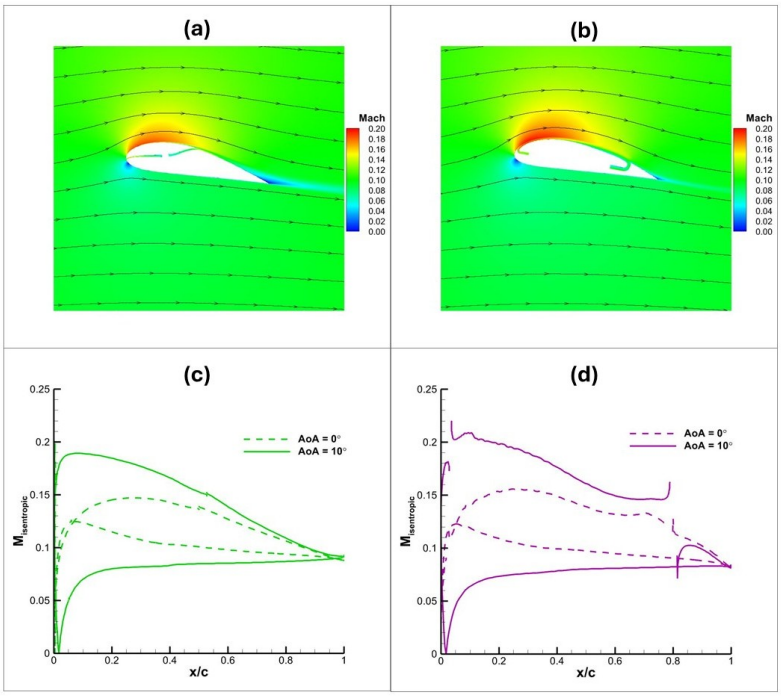

Figure 8: Flow field and corresponding isentropic Mach number surface plot for 2D AFC3 and AFC4 for $\alpha = 10°$

Given that the area enclosed by the isentropic Mach number plot of AFC4 at $\alpha = 10°$ is notably larger than that of the other AFC configurations, it might be expected that C_L would also be significantly greater due to the high circulation; however, this is not observed in Figure 9a. This is explained by Figure 11d in that the contribution of the pressure force (airfoil circulation) to lift is the highest in AFC4, but the effect of the suction reduces the overall C_L. The large suction contribution is due to the slot being oriented mostly in the streamwise direction. These effects can be mitigated by the slot being oriented more towards the transverse direction as done by Liu and Zha[57]. For AFC1 and AFC2, in Figure 10e and Figure 10f respectively, the circulation contribution is significantly lower than AFC4, but the jet reactionary force near perfectly cancels the C_L reduction by the suction slot such that the resulting lift and drag plot traces the pressure contribution plot. The position and orientation of the suction and injection slots of AFC3 in Figure 11c did not allow for this compensating behavior. The suction slot at the LE causes the flow to be reduced and diverted from the suction surface, reducing the pressure contribution to lift and increasing the drag. This can be seen in the reduced suction peak of AFC3 in Figure 8a and the C_L being lower than the NACA6421 airfoil in Figure 9a at low AoA. As AoA increases, the injection contribution compensates for the loss in the pressure contribution.

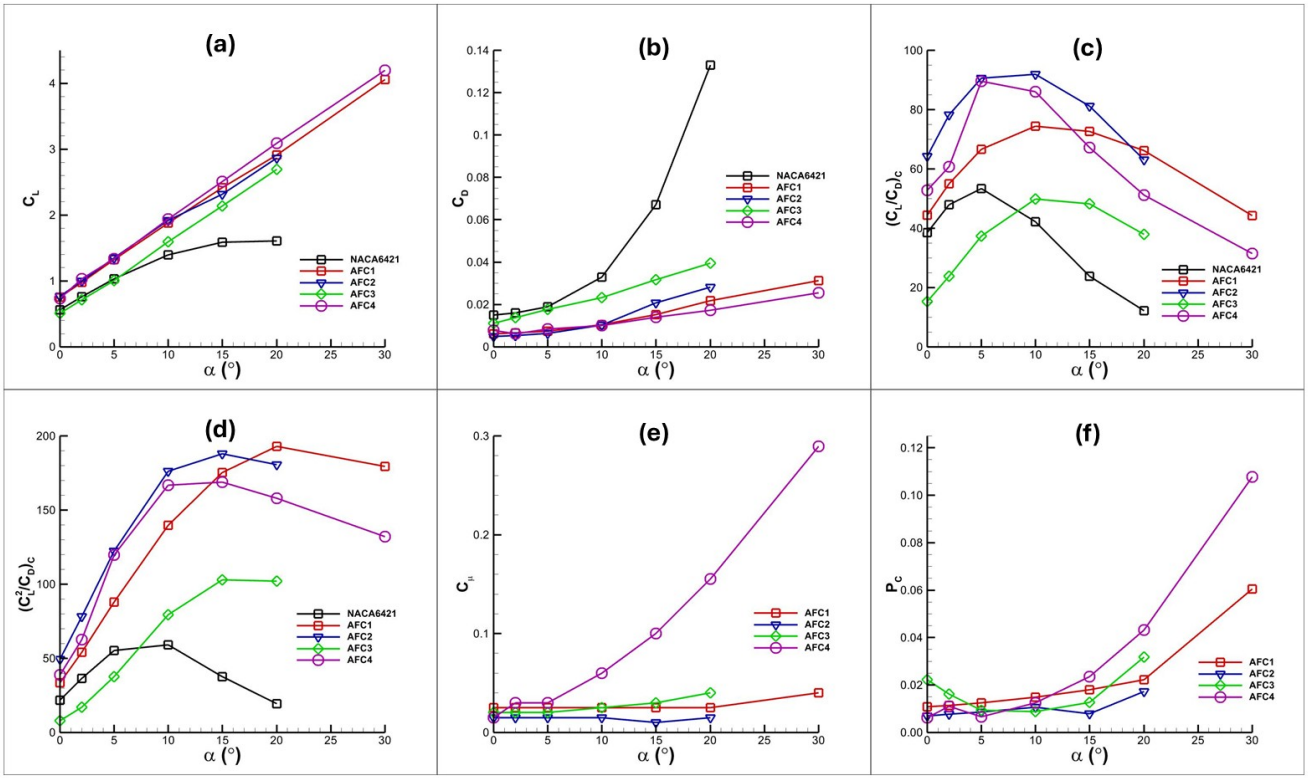

Figure 9: 2D AFC airfoil performance versus AoA

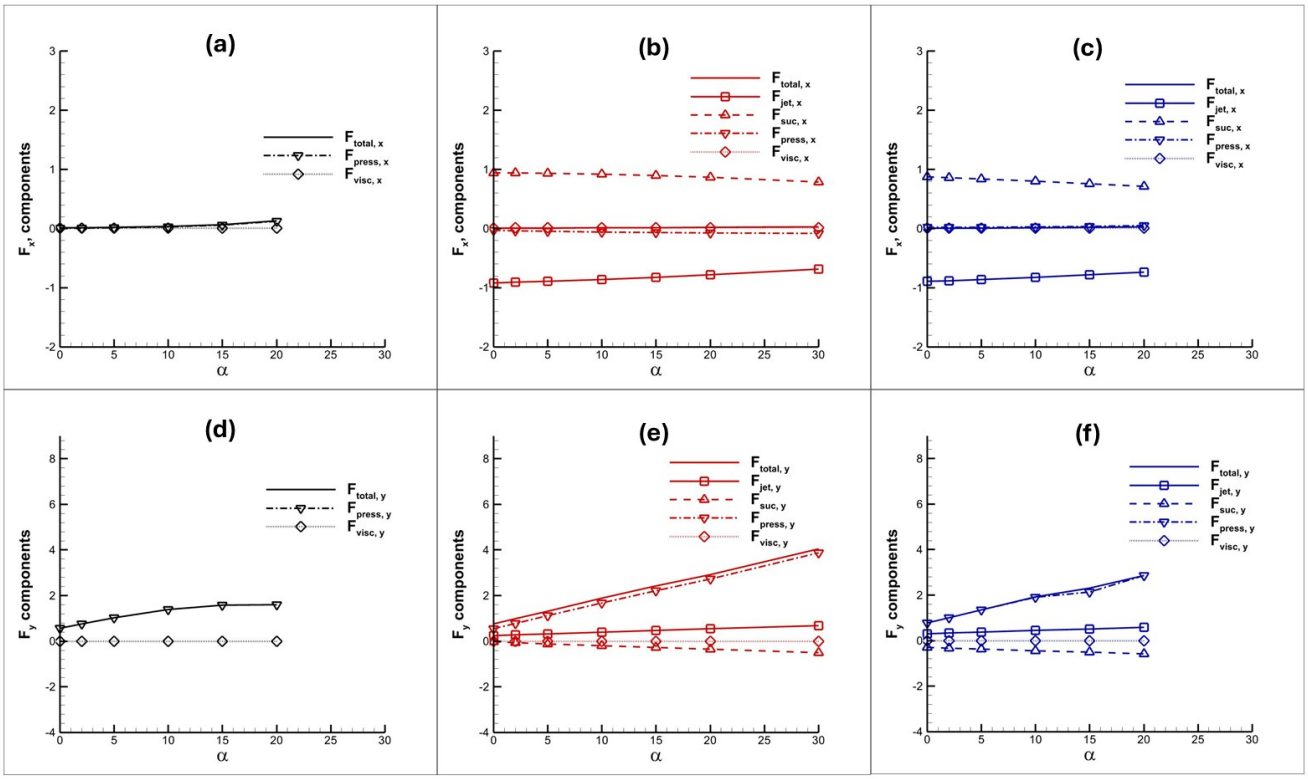

Figure 10: Force component analysis for 2D NACA6421, AFC1 and AFC2 airfoils

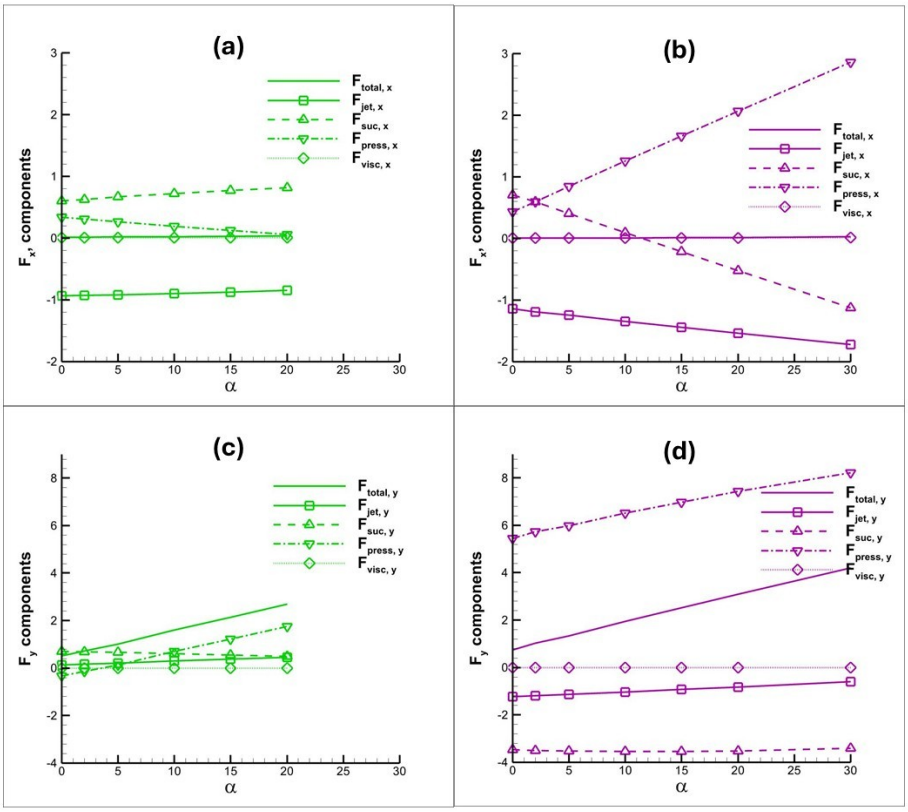

Figure 11: Force component analysis for 2D AFC3 and AFC4 airfoils

All AFC configurations are able to extend the stall margin beyond the stall point of the NACA6421 as seen in Figure 9. However, it is noted that after $\alpha = 20°$ both AFC2 and AFC3 are unable to produce a converged result and are hence omitted. A similar trend to C_L is observed for C_D although there is a greater deviation in the values from $\alpha = 10°$ onward. AFC3 has a noticeable larger drag due to the aforementioned reason. The maximum aerodynamic efficiency is achieved by AFC2 achieving a maximum value of $(C_L/C_D)_c = 91.91$ at $\alpha = 10°$ and maintains a higher aerodynamic efficiency until $\alpha = 20°$. AFC4 peaks around $\alpha = 5°$ achieving a value of $(C_L/C_D)_c = 89.56$ and AFC1 peaks around $\alpha = 10°$ achieving a value of $(C_L/C_D)_c = 74.34$. Similarly, in terms of airfoil productivity, AFC2 maintains a higher productivity peaking at $\alpha = 15°$ with a value of $(C_L^2/C_D)_c = 187.90$. Subsequently, AFC1 increases beyond AFC2, achieving a maximum airfoil productivity of $(C_L^2/C_D)_c = 192.93$ at $\alpha = 20°$. AFC4 peaks around $\alpha = 10°$. Although AFC4 has larger C_L and lower C_D values beyond $\alpha = 15°$, the corresponding P_C values increase more rapidly and decrease its efficiency, as seen in Figure 9f. The tabulated performance result of each AFC configuration is given in Table 6 in the appendix.

Generally, the CFJ is capable of maintaining a lower P_C value due to injection into a low static pressure region and suction from a high static pressure region. However, examining it on the basis of C_μ, increasing the AoA requires a higher input of C_μ, which after the lower AoA, makes P_C grow correspondingly. For all configurations that contain the injection duct downstream of the suction duct, namely AFC1, AFC2 and AFC3, although not located in the most efficient locations to apply suction and injection, as with AFC4, due to the effectiveness of using the injected air stream to energize the flow and for reattachment, a reduction of required C_μ could be achieved. This reduces the resulting P_C for these configurations, as seen in Figure 9f. Of these configurations, AFC2 requires the lowest C_μ and consequently relatively low P_C values, while still maintaining a similar C_L within its stall margin. This is likely as a result of the

positioning of the suction and injection slots. Possibly having the injection slot in the vicinity of the TE reduces the C_μ required to reattach the flow to the TE. However, the exact reasoning for the reduced C_μ resulting from the slot arrangement and positioning is not well understood at this time. This behavior is opposed to AFC1, which is at or near the suction peak location, depending on the AoA, and would hence require more power to withdraw air in that region. However, at higher AoA, such as $\alpha = 20°$ or $30°$, the suction peak shifts upstream and the suction slot would be significantly downstream such that it behaves similarly to AFC2 at lower AoA. This may be the reason why AFC1 has a higher aerodynamic and airfoil productivity at high AoA as seen in Figures 9c and 9d.

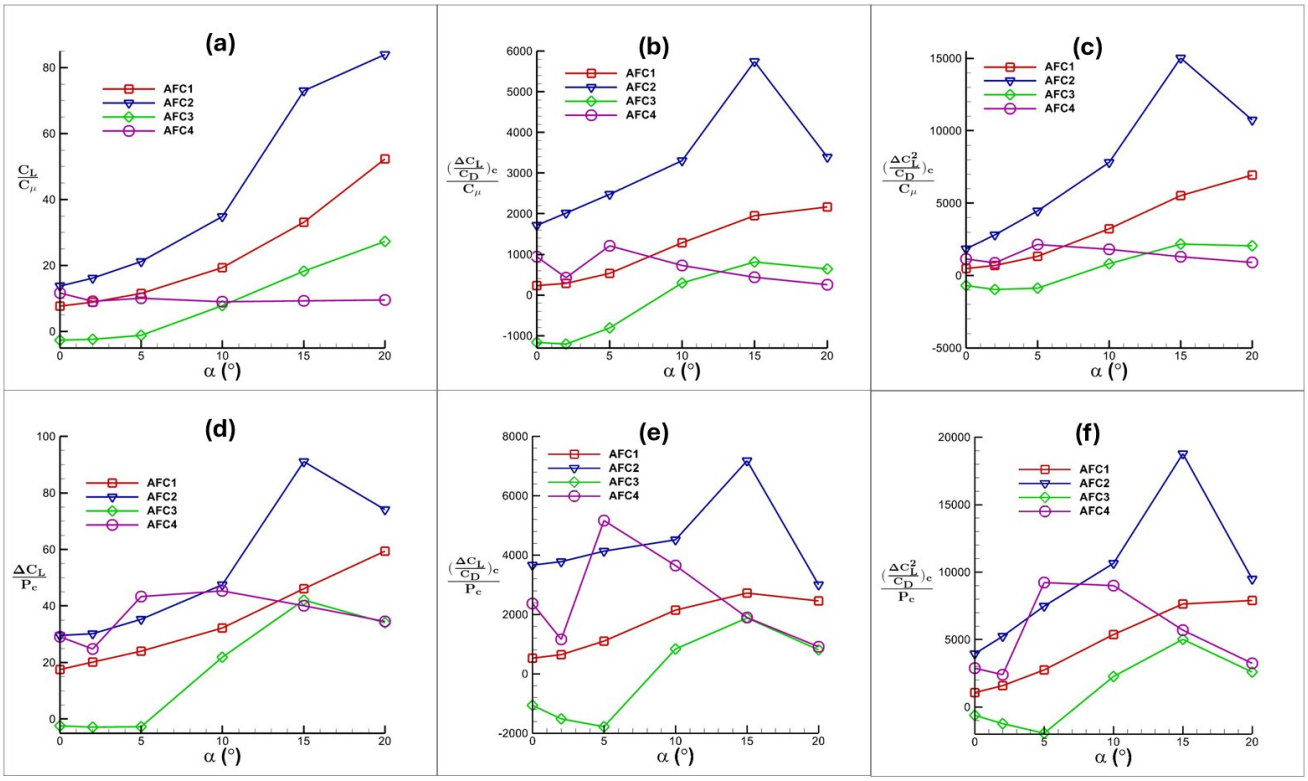

Figure 12: 2D AFC airfoil performance increase per C_μ and per P_C versus AoA

Figure 12 provides details on the effectiveness and efficiency of the different AFC airfoils over the baseline NACA6421 airfoil. $\Delta C_L/C_\mu$, often referred to as the lift gain factor, indicates the additional lift generated per unit of jet momentum supplied, given by C_μ, from the use of AFC. It is one of the indicators of effectiveness. It can be seen in Figure 12a that AFC2 consistently has the largest lift gain factor for all AoA and can be interpreted as the most effective in increasing C_L per C_μ supplied. AFC1 is the next most effective in increasing C_L, except at $\alpha = 0°$. The lift gain factor of these airfoils increase steadily with AoA. Interestingly, AFC4 has a very consistent lift gain factor regardless of AoA as seen in Figure 12a and is related to C_L increasing steadily with C_μ as seen in Figures 9a and 9e. It is also noted that AFC3 has a negative lift gain factor up to $\alpha = 5°$, meaning that for low AoA, AFC3 is less effective than the baseline NACA6421 airfoil. Figures 12b and 12c have similar trends, although the plot of AFC4 is no longer near level but peaks at $\alpha = 5°$ and AFC2 has a noticeable performance decrease at $\alpha = 20°$. These trends in the effectiveness plots can be explained by Figure 9.

In terms of efficiency measured as the performance gain per unit power required, Figures 12d, 12e, and 12f all share similar trends. Initially, AFC2 is most efficient in increasing the different aerodynamic

parameters until $\alpha = 5°$ at which point AFC4 peaks above AFC2 before steadily declining. For the remaining AoA, AFC2 remains the most efficient, but AFC2 has small stall margin and is unable to attach the flow at AoA higher than 20°. AFC1 initially has a lower efficiency in increasing the different parameters, but steadily increases towards $\alpha = 15°$, at which point AFC4 is surpassed. AFC3 starts with negative values, indicating that it is less efficient to increase the different AFC parameters compared to the baseline NACA6421 airfoil up to $\alpha = 5°$.

6 Conclusion

This paper presents the numerical investigation of four (4) 2D active flow control (AFC) airfoils compared to a baseline NACA6421 airfoil under cruise conditions. The AFC airfoils are assessed based on effectiveness and power requirements. The prescribed jet momentum coefficient, C_μ, is set based on the value that would produce the highest aerodynamic efficiency, $(C_L/C_D)_c$, for a given AoA. All AFC configurations are able to extend the stall margin above the baseline NACA6421 airfoil, though to different extents. Having the suction slot downstream from the suction peak appears to demonstrate lower power requirements such as in AFC2 and AFC4 compared to near the suction peak in AFC1. AFC4 demonstrates the highest circulation enhanced lift augmentation, although the position and orientation of the suction slot significantly reduces the lift increment. AFC airfoils with the injection slot downstream of the suction slot appear to benefit significantly from the jet reactionary force, although the extent to which may be dependent on the proximity to the suction slot and the TE. Of the airfoils in this investigation. AFC2 achieves the highest aerodynamic efficiency of $(C_L/C_D)_c = 91.91$ at $\alpha = 10°$, AFC4 has a slightly lower value of 89.56. Both AFC2 and AFC4 peak at relatively lower AoA of $\alpha = 10°$ and $\alpha = 5°$, respectively, before gradually reducing in efficiency. The higher aerodynamic efficiency of AFC1 at $\alpha = 20°$ and $\alpha = 30°$ is likely due to the movement of the suction peak upstream and causing it to behave similar to AFC2 at a lower AoA. This delayed increase in efficiency also results in a delayed peak in airfoil productivity achieving a maximum of $(C_L^2/C_D)_c = 192.93$ at $\alpha = 20°$ for AFC1. AFC2 demonstrates the highest effectiveness gain over the baseline NACA6421. It also has the highest efficiency gain, except at $\alpha = 5°$ at which point AFC4 peaks before steadily declining. AFC1 steadily increases in both effectiveness gain and efficiency gain until $\alpha = 15°$. However, AFC3 is less effective and efficient than the baseline NACA6421 airfoil until $\alpha = 10°$. Since the AFC airfoil could be sensitive to the slot sizes, locations, and orientation, this study is based on limited trade studies and should be used as a preliminary reference instead of definitive conclusions.

7 Acknowledgment

The University of Miami is acknowledged for their support for sponsoring the Dean's Fellowship. The computing resource for this simulation is provided by CoFlow Jet, LLC.

Disclosure: The University of Miami and Dr. Gecheng Zha may receive royalties for future commercialization of the intellectual property used in this study. The University of Miami is also equity owner in CoFlow Jet, LLC, licensee of the intellectual property used in this study.

References

[1] Gad-El-Hak, Mohamed, *Separation Control*, pp. 150–188. Cambridge, United Kingdom: Cambridge Univeristy Press, 2000.

[2] B. Dillner, F. W. May, and J. H. McMasters, "Aerodynamic Issue in the Design of High-Lift Systems for Transport Aircraft," in *Proceedings of the Conference on Improvement ot Aerodynamic Performance through Boundary Layer Control and High Lift Systems Held at the Fluid Dynamics Panel Symposium*, (Brussels, Belgium), Advisory Group for Aerospace Research and Development(AGARD), 1984.

[3] A. S. W. Thomas, "Aircraft Drag Reduction Technology - A Summary." Advisory Group for Aerospace Research and Development, AGARD Report No.723, 1985.

[4] D. J. Butter, "Recent Progress on Development and Understanding of High Lift Systems," in *Proceedings of the Conference on Improvement ot Aerodynamic Performance through Boundary Layer Control and High Lift Systems Held at the Fluid Dynamics Panel Symposium*, (Brussels, Belgium), Advisory Group for Aerospace Research and Development(AGARD), 1984.

[5] Campbell, J. P., "Overview of Powered-Lift Technology." NASA. Langley Res. Center Powered-Lift Aerodyn. and Acoustics, Accession Number: 78N24047, 1976.

[6] Prandtl, Ludwig, "Motion of fluids with very little viscosity." NACA Technical Memorandum 452, January 1928.

[7] P. Poisson-Quinton, "Recherches theoriques et experimentales sur le controle de couche limites," in *Congress of Applied Mechanics, London*, 1948.

[8] Englar, Robert J., "Development of the A-6/Ciculation Control Wing Flight Demonstrator Configuration." Final Report, January 1979.

[9] Yang, Yunchao and Zha, Gecheng, "Super-Lift Coefficient of Active Flow Control Airfoil: What is the Limit?," *AIAA Paper 2017-1693, AIAA SCITECH2017, 55th AIAA Aerospace Science Meeting, Grapevine, Texas, 9-13 January 2017*, 2017.

[10] H. Schlichting and K. Gersten, *Boundary-Layer Theory*. Springer Nature, 2017.

[11] M. Amitay, D. R. Smith, V. Kibens, D. E. Parekh, and A. Glezer, "Aerodynamic flow control over an unconventional airfoil using synthetic jet actuators," *AIAA Journal*, vol. 39, no. 3, pp. 361–370, 2001.

[12] M. L. Post and T. C. Corke, "Separation control using plasma actuators: Dynamic stall vortex control on oscillating airfoil," *AIAA Journal*, vol. 44, no. 12, pp. 3125–3135, 2006.

[13] P. Scholz, M. Casper, J. Ortmanns, C. J. Kähler, and R. Radespiel, "Leading-edge separation control by means of pulsed vortex generator jets," *AIAA Journal*, vol. 46, no. 4, pp. 837–846, 2008.

[14] E. Whalen, M. Spoor, P. Vijgen, J. Tran, A. Shmilovich, J. Lin, and M. Andino, "Full-scale flight demonstration of an active flow control enhanced vertical tail," 06 2016.

[15] Kewei Xu, Gecheng Zha, "Enhancing aircraft control surface effectiveness by co-flow jet flap at low energy expenditure," *Elsevier Journal of Aerospace Science and Technology 133 (2023) 108145, https://doi.org/10.1016/j.ast.2023.108145*, 2023.

[16] D. Greenblatt, E. A. Whalen, and I. J. Wygnanski, "Introduction to the flow control virtual collection," *AIAA Journal*, vol. 57, pp. 3111–3645, 2019.

[17] K. Xu, Y. Ren, and G. Zha, *Numerical Analysis of Energy Expenditure for Co-Flow Wall Jet Separation Control*. American Institute of Aeronautics and Astronautics, 2022.

[18] Xu, Kewei and Ren, Yan and Zha, Gecheng, "Numerical Analysis of Energy Expenditure for Co-Flow Wall Jet Separation Control," *AIAA Paper 2022-1547, AIAA Scitech Forum, January 3-7*, 2022.

[19] Lefebvre, A. and Zha, G.-C., "Design of High Wing Loading Compact Electric Airplane Utilizing Co-Flow Jet Flow Control." AIAA Paper 2015-0772, AIAA SciTech2015: 53nd Aerospace Sciences Meeting, Kissimmee, FL, 5-9 Jan 2015.

[20] A. Lefebvre, B. Dano, W. B. Bartow, M. D. Fronzo, and G. C. Zha, "Performance and energy expenditure of coflow jet airfoil with variation of mach number," *Journal of Aircraft*, vol. 53, no. 6, pp. 1757–1767, 2016.

[21] G.-C. Zha and D. C. Paxton, "A Novel Flow Control Method for Airfoil Performance Enhancement Using Co-Flow Jet." *Applications of Circulation Control Technologies*, Chapter 10, p. 293-314, Vol. 214, Progress in Astronautics and Aeronautics, AIAA Book Series, Editors: Joslin, R. D. and Jones, G.S., 2006.

[22] Wang, Yang and Zha, Gecheng, "Study of Reynolds Number Effect for Co-Flow Jet Airfoil/Wing," *AIAA Paper 6.2020-2666, AIAA Aviation 2020 Forum, June 15-19, 2020, Virtual Event*, 2020.

[23] T. Zengjunz, D. Huishen, L. Peiqing, C. Jianzhong, and H. Yuwei, "Wing structure having lamellar flow flowing control and separation control," August 2010. CN2008101194795A.

[24] Gainer, Thomas G. and Yip, Long P. and Vogler, Raymond D., "Comparison of aerodynamic theory and experiment for jet-flap wings." Powered-Lift Aerodynamics and Acoustics, Accession Number: 78N24052, January 1976.

[25] A. T. Perry and P. J. Ansell, "Crossflow fan power requirements for boundary-layer suction in transonic flow," *Journal of Aircraft*, vol. 54, no. 3, pp. 1217–1220, 2017.

[26] Kim, Hyun D. and Saunders, John D., "Embedded Wing Propulsion Conceptual Studyl." NASA/TM—2003-212696, November 2003.

[27] G.-C. Zha, W. Gao, and C. Paxton, "Jet Effects on Co-Flow Jet Airfoil Performance," *AIAA Journal, No. 6,*, vol. 45, pp. 1222–1231, 2007.

[28] G.-C. Zha, C. Paxton, A. Conley, A. Wells, and B. Carroll, "Effect of Injection Slot Size on High Performance Co-Flow Jet Airfoil," *AIAA Journal of Aircraft*, vol. 43, 2006.

[29] G.-C. Zha, B. Carroll, C. Paxton, A. Conley, and A. Wells, "High Performance Airfoil with Co-Flow Jet Flow Control," *AIAA Journal*, vol. 45, 2007.

[30] Wang, B.-Y. and Haddoukessouni, B. and Levy, J. and Zha, G.-C., "Numerical Investigations of Injection Slot Size Effect on the Performance of Co-Flow Jet Airfoil," *Journal of Aircraft*, vol. Vol. 45, No. 6,, pp. pp.2084–2091, 2008.

[31] B. P. E. Dano, D. Kirk, and G.-C. Zha, "Experimental Investigation of Jet Mixing Mechanism of Co- Flow Jet Airfoil." AIAA-2010-4421, 5th AIAA Flow Control Conference, Chicago, IL, 28 Jun - 1 Jul 2010.

[32] B. P. E. Dano, G.-C. Zha, and M. Castillo, "Experimental Study of Co-Flow Jet Airfoil Performance Enhancement Using Micro Discreet Jets." AIAA Paper 2011-0941, 49th AIAA Aerospace Sciences Meeting, Orlando, FL, 4-7 January 2011.

[33] A. Lefebvre, B. Dano, W. Bartow, M. Fronzo, and G. Zha, "Performance and energy expenditure of coflow jet airfoil with variation of mach number," *Journal of Aircraft*, vol. 53, no. 6, pp. 1757–1767, 2016.

[34] A. Lefebvre, G-C. Zha, "Numerical Simulation of Pitching Airfoil Performance Enhancement Using Co-Flow Jet Flow Control," *AIAA paper 2013-2517*, June 2013.

[35] A. Lefebvre, G-C. Zha, "Cow-Flow Jet Airfoil Trade Study Part I : Energy Consumption and Aerodynamic Performance," *Proceedings of the AIAA Flow Control Conference*, June 2014.

[36] A. Lefebvre, G-C. Zha, "Cow-Flow Jet Airfoil Trade Study Part II : Moment and Drag," *Proceedings of the AIAA Flow Control Conference*, June 2014.

[37] Zha, Gecheng and Yang, Yunchao and Ren, Yan and McBreen, Brendan, "Super-Lift and Thrusting Airfoil of Coflow Jet Actuated by Micro-Compressors," *AIAA Paper-2018-3061, AIAA AVIATION Forum 2018, Flow Control Conference, June 25-29*, 2018.

[38] Lefebvre, A. and Zha, G.-C., "Trade Study of 3D Co-Flow Jet Wing for Cruise Performance." AIAA Paper 2016-0570, AIAA SCITECH2016, AIAA Aerospace Science Meeting, San Diego, CA, 4-8 January 2016.

[39] Xu, Kewei and Zha, Gecheng, "High Control Authority 3D Aircraft Control Surfaces Using Co-Flow Jet," *AIAA Journal of Aircraft*, 2020.

[40] Xu, Kewei and Ren, Yan and Zha, Gecheng, "Numerical Analysis of Energy Expenditure for Co-Flow Wall Jet Separation Control," *AIAA Journal, published online: 11 Jan 2022, doi.org/10.2514/1.J061015*, 2022.

[41] B. McBreen, K.-W. Xu, G.-C. Zha, "Numerical Study of Extreme Adverse Pressure Gradients Enabled by Co-Flow Jet," *AIAA Paper-2023-1430, AIAA SCITECH 2023 Forum, 23-27 January 2023, National Harbor, MD*, 2023.

[42] B. McBreen, Y.-C. Yang, G.-C. Zha, "Improved Delayed Detached Eddy Simulation of Co-Flow Jet Flow Control in Extreme Adverse Pressure Gradients," *AIAA paper 2024-0063, AIAA SCITECH 2024 Forum, 8-12 January 2024, Orlando, FL*, 2024.

[43] F. Ding, J. Jeon, and G. Zha, "Trade study of regular and flapped coflow jet airfoils," *AIAA Journal*, 2026.

[44] Y.-Q. Shen and G.-C. Zha, "Large Eddy Simulation Using a New Set of Sixth Order Schemes for Compressible Viscous Terms ," *Journal of Computational Physics*, vol. 229, pp. 8296–8312, 2010.

[45] Zha, G.C., Shen, Y.Q. and Wang, B.Y., "An improved low diffusion E-CUSP upwind scheme ," *Journal of Computer and Fluids*, vol. 48, pp. 214–220, Sep. 2011.

[46] Y.-Q. Shen and G.-Z. Zha , "Generalized finite compact difference scheme for shock/complex flowfield interaction," *Journal of Computational Physics*, vol. doi:10.1016/j.jcp.2011.01.039, 2011.

[47] Shen, Y.-Q. and Zha, G.-C. and Wang, B.-Y., " Improvement of Stability and Accuracy of Implicit WENO Scheme," *AIAA Journal*, vol. 47, No. 2, pp. 331–344, 2009.

[48] Shen, Y.-Q. and Zha, G.-C. and Chen, X.-Y., " High Order Conservative Differencing for Viscous Terms and the Application to Vortex-Induced Vibration Flows," *Journal of Computational Physics*, vol. 228(2), pp. 8283–8300, 2009.

[49] Shen, Y.-Q. and Zha, G.-C. , " Improvement of the WENO Scheme Smoothness Estimator," *International Journal for Numerical Methods in Fluids*, vol. DOI:10.1002/fld.2186, 2009.

[50] G.-C. Zha and E. Bilgen, "Numerical Study of Three-Dimensional Transonic Flows Using Unfactored Upwind-Relaxation Sweeping Algorithm," *Journal of Computational Physics*, vol. 125, pp. 425–433, 1996.

[51] B.-Y. Wang and G.-C. Zha, "A General Sub-Domain Boundary Mapping Procedure For Structured Grid CFD Parallel Computation," *AIAA Journal of Aerospace Computing, Information, and Communication*, vol. 5, No.11, pp. 2084–2091, 2008.

[52] Wang, B Y and Zha, G.-C., "Detached-Eddy Simulation of a Co-Flow Jet Airfoil at High Angle of Attack," *AIAA Journal of Aircraft*, vol. 48, 5, pp. 1495–1502, 2011.

[53] Im, H.-S. and Zha, G.-C. and Dano, B. P. E., "Large Eddy Simulation of Coflow Jet Airfoil at High Angle of Attack," *Journal of Fluid Engineering, vol. 136(2), p. 021101*, 2014.

[54] Lefebvre, A. and Dano, B. and Bartow, W. and DiFranzo, M. and Zha, G.-C., "Performance and Energy Expenditure of Co-Flow Jet Airfoil with Variation of Mach Number," *Journal of Aircraft, Vol. 53, No. 6, Nov-Dec. 2016, pp.1757-1767*, 2016.

[55] K. Xu, Y. Ren, and G. Zha, "Analysis of separation control mechanism of turbulent co-flow wall jet," *Aerospace Science and Technology*, vol. 168, p. 110775, 2026.

[56] Y.-Q. Shen, G.-C. Zha, and B.-Y. Wang, "Improvement of Stability and Accuracy of Implicit WENO Scheme ," *AIAA Journal*, vol. 47, pp. 331–344, 2009.

[57] Z. Liu and G. Zha, "Transonic airfoil performance enhancement using co-flow jet active flow control," *AIAA Journal*, 2016.

A Appendix

Table 5: NACA 6421 Baseline Results

AoA	C_L	C_D	C_L/C_D	C_L^2/C_D
0°	0.561	0.015	38.550	21.620
2°	0.759	0.016	47.986	36.403
5°	1.032	0.019	53.393	55.111
10°	1.396	0.033	42.256	58.990
15°	1.587	0.067	23.764	37.704
20°	1.607	0.133	12.113	19.466

Table 6: 2D AFC Results

Identifier	AoA	C_μ	C_L	C_D	C_L/C_D	Γ	P_c	$(C_L/C_D)_c$	$(C_L^2/C_D)_c$
	0°	0.025	0.753	0.006	122.298	1.008	0.011	44.416	33.429
	2°	0.025	0.981	0.006	151.637	1.009	0.011	55.063	53.996
	5°	0.025	1.321	0.006	179.813	1.010	0.012	66.624	87.981
AFC1	10°	0.025	1.880	0.010	180.558	1.012	0.015	74.340	139.770
	15°	0.025	2.415	0.015	180.558	1.014	0.018	72.583	175.301
	20°	0.025	2.913	0.022	133.577	1.017	0.022	66.222	192.934
	30°	0.040	4.054	0.031	130.024	1.038	0.060	44.234	179.311
	0°	0.015	0.767	0.005	155.810	1.007	0.007	64.210	49.272
	2°	0.015	1.001	0.005	192.842	1.008	0.008	78.251	78.321
	5°	0.015	1.350	0.006	213.256	1.009	0.009	90.608	122.284
AFC2	10°	0.015	1.918	0.010	186.945	1.011	0.011	91.908	176.283
	15°	0.010	2.315	0.021	111.758	1.010	0.008	81.153	187.899
	20°	0.015	2.866	0.028	101.525	1.017	0.017	63.041	180.671
	30°	-	-	-	-	-	-	-	-
	0°	0.020	0.507	0.011	45.744	1.019	0.022	15.228	7.728
	2°	0.020	0.712	0.014	51.751	1.014	0.016	23.799	16.934
	5°	0.020	1.007	0.018	56.822	1.008	0.009	37.288	37.566
AFC3	10°	0.025	1.592	0.023	68.360	1.007	0.009	49.812	79.314
	15°	0.030	2.135	0.032	67.477	1.009	0.013	48.264	103.030
	20°	0.040	2.696	0.039	68.307	1.020	0.032	37.858	102.061
	30°	-	-	-	-	-	-	-	-
	0°	0.015	0.736	0.008	94.899	1.005	0.006	52.751	38.826
	2°	0.030	1.031	0.006	169.696	1.006	0.011	60.744	62.645
	5°	0.030	1.335	0.008	161.030	1.004	0.007	89.564	119.612
AFC4	10°	0.060	1.939	0.010	191.104	1.005	0.012	86.014	166.795
	15°	0.100	2.509	0.014	181.114	1.007	0.023	67.225	168.686
	20°	0.155	3.088	0.017	178.978	1.010	0.043	51.130	157.893
	30°	0.290	4.196	0.026	164.543	1.019	0.108	31.481	132.109